Nuclear Physics A462 (1987) 1-25
North-Holland, Amsterdam

CORE POLARIZATION EFFECTS ON TRANSITION DENSITIES IN MEDIUM-HEAVY NUCLEI

H. SAGAWA[1], O. SCHOLTEN[2] and B.A. BROWN

National Superconducting Cyclotron Laboratory, Michigan State University, East Lansing, Michigan 48824-1321, USA

B.H. WILDENTHAL

Department of Physics and Atmospheric Science, Drexel University, Philadelphia, Pennsylvania 19104, USA

Received 23 June 1986

Abstract. We propose a microscopic model to study the core-polarization effects of giant resonances on the transition densities of open-shell nuclei. We use the Hartree-Fock-RPA method for the calculation of the single-particle wave functions and the response function of the giant resonances. Particle-vibration coupling is applied to take into account the core polarization effect on the valence many-body wave functions. We apply our model to the quadrupole transitions in the several medium-heavy nuclei. Valence many-body wave functions are calculated with the generalized seniority scheme and with the shell model. Results for the proton and neutron effective charges and the Coulomb form factors for the $N = 82$ isotones and for ^{116}Sn and ^{110}Pd are presented and discussed. The effective coupling hamiltonian is determined by the Skyrme interaction SGII which is used also in the HF and RPA calculations. The calculated core polarization charges show some state dependences. The average theoretical values are $\delta e_p = 0.4$-0.5 and $\delta e_n = 0.6$-0.7 compared to typical empirical values of $\delta e_p = 0.6$ and $\delta e_n = 1.2$.

1. Introduction

Recent progress in electron scattering experiments has given us precise information about the transition densities and current densities of collective states of nuclei over a wide region of the mass table [1]). These data are especially useful for distinguishing the validities of various nuclear models. Transition amplitudes to low-excited states in light nuclei have been calculated by using the shell model [2-4]) and the random phase approximation [5]). While these models can describe fairly well the excitation energies of collective states, the theoretical transition strengths are usually much smaller than the experimental ones (typically a factor of 4 in the sd-shell nuclei). Empirically this has been taken care of by introducing "effective charges" for protons and neutrons. In light nuclei, their magnitudes have been qualitatively understood by *the coherent mixing of the 1p-1h giant resonances into the low-lying states* [6-8]). This is often referred to as *the core-polarization effect.*

[1] Present address: Department of Physics, Faculty of Science, University of Tokyo, Hongo 7-2-1, Bunkyo-ku Tokyo 113, Japan.

[2] Present address: KVI, Zernikelaan 25, 9747 AA Groningen, The Netherlands.

A microscopic model has recently been applied to the study of the core polarization effect on the transition and current densities of the single-particle configurations [8]). This model consists of two parts. First, the spherical single-particle wave functions are calculated by the self-consistent Hartree-Fock (HF) method and the strength distributions of the giant resonances are calculated by the RPA method. Then, the core polarization effect on the single-particle electromagnetic transition amplitude is evaluated using the particle-vibration coupling model [6]). In our model, the key and the only ingredient for all of the calculations is a unified nuclear effective interaction. The hamiltonian for the particle-vibration coupling is the same Skyrme-type interaction as used in the HF and RPA calculations. We used the parameter set SGII [9]) which was designed to successfully reproduce many of the ground-state and giant-resonance-state properties of the closed-shell nuclei over a wide mass region. Previous work on the calculations of core-polarization effects have used finite-range two-body interactions [7]) or schematic two-body interactions [10]). Our model successfully describes not only the absolute magnitude of the E2 and E4 core-polarization charges determined empirically for the sd-shell configurations but also the q-dependence of the electron scattering Coulomb form factors [8,11]).

In medium-heavy nuclei, many theoretical models have been used to describe the transition densities of the low-lying collective excitations; the shell-model [12]), the RPA [13]) and the interacting boson model (IBM) [14].) While each model is fairly successful in reproducing the energy spectra of those nuclei, the theoretical transition strengths are again much smaller than the experimental ones (since the IBM model is a macroscopic phenomenological model, we cannot calculate the absolute magnitude of the transition strength within that model. However, microscopic calculations which try to justify the IBM mapping also require effective charges in order to obtain quantitative agreement with the experimental transition strengths [14])). In general, the empirical E2 effective charges for medium-heavy nuclei ($\delta e_p \simeq \delta e_n \approx 1$) are much larger than those of light nuclei ($\delta e_p \approx \delta e_n \approx 0.4$). Although the origin of the effective charge in medium-heavy nuclei has been studied in the macroscopic model [6]), much remains to be understood at the microscopic level. In this paper, we will study the E2 core-polarization charges and C2 form factors of medium-heavy nuclei based on a fully microscopic model.

We adopt the generalized seniority scheme in order to calculate identical particle many-body wave functions in medium-heavy nuclei [15,16]). The configuration space for this calculation is limited to several single-particle states (usually within $0\hbar\omega$) around the Fermi surface. In some nuclei, we will compare results of the generalized seniority scheme with large-scale shell-model calculations carried out with a phenomenological effective interaction [12]). The core polarization for the many-body wave functions is taken into account by an extension of the single-particle-vibration coupling model [11]). The generalized seniority scheme and shell-model calculations are described in sect. 2. The formulation for the core polarization of the many-body wave function is given in sect. 3. The numerical results for the $N = 82$ isotones and

the Sn isotopes are discussed in sects. 4.1–4.3. As an example of a mixed proton-neutron system, we have carried out calculations for ^{110}Pd within the framework of IBA-2, these results are discussed in sect. 4.4. The summary is given in sect. 5.

2. Microscopic calculations of the valence many-body wave functions

2.1. THE GENERALIZED SENIORITY SCHEME

The dominant problem in shell-model calculations for medium and heavy nuclei is the large size of the configuration spaces. Even if calculations are restricted to semi-closed shell nuclei, for which only one kind of particle is active, the dimensions of the configuration spaces are easily of the order of several thousands or more for the $J=2$ state near the middle of the shell. In order to simplify the calculation, Talmi [15]) proposed a model which is a generalization of the seniority scheme (the so-called generalized seniority scheme) and this model has been useful for describing semi-magic nuclei.

First we will briefly describe the generalized seniority scheme as used in the present calculation [16]). Let us consider a state of two particles with $J=0$ distributed over several j-orbits. Such a state can be obtained by operating with the creation operator

$$S_+ = \sum_j \alpha_j S_{+j}, \tag{1}$$

with

$$S_{+j} = \sum_m (-)^{j-m} a^\dagger_{jm} a^\dagger_{j-m} \tag{2}$$

on the closed shell, which acts as a vacuum. The S_{+j} operator creates a $J=0$ state in the j^2 configuration. It is one of the quasi-spin operators, and is a generator of the SU(2) Lie algebra, together with

$$S_{-j} = (S_{+j})^\dagger, \tag{3}$$

$$S_{zj} = \tfrac{1}{2}[\hat{n}_j - \tfrac{1}{2}(2j+1)] = \tfrac{1}{2}(\hat{n}_j - \Omega), \tag{4}$$

where $\hat{n}_j$ is the number operator. The different irreducible representations can be labeled with the quasi-spin and its z component, S_z, or alternately with the seniority v and n the number of particles in the orbit. The two sets of labels are related via

$$S = \tfrac{1}{2}(\Omega - v) \qquad \text{and} \qquad S_z = \tfrac{1}{2}(n - \Omega). \tag{5}$$

The seniority quantum number thus measures the number of unpaired particles in the j-orbit. In the case of a multi-j shell, with arbitrary coefficients α_j, the S_+ operator defined in eq. (1) cannot be combined with its adjoint,

$$S_- = \sum_j \alpha_j S_{-j} \tag{6}$$

to generate an SU(2) algebra. The direct contact with an underlying group symmetry is thus lost. This causes complications in deriving reduction formulae for one- and two-body matrix elements.

The absence of a group symmetry prevents the introduction of a good quantum number, but it is still possible to introduce a label, ν, the generalized seniority for the states. In analogy to seniority, it is defined according to the following prescription. First, a state with the seniority $\nu = 0$ is defined by

$$|\tilde{j}^n \nu = 0, J = 0\rangle = S_+^N |0\rangle / K, \tag{7}$$

where $\tilde{j}^n$ implies a state with n particles in a multi-j shell configuration, $N = \frac{1}{2}n$ and K is a normalization factor. The state with $\nu = 2$ can be defined as

$$|\tilde{j}^n \nu = 2, J\rangle = S_+^{N-1} |\tilde{j}^2 J\rangle / K' . \tag{8}$$

Notice that in the case of a multi-j shell we can construct a $J = 0$ state with the seniority $\nu = 2$ by choosing $|\tilde{j}^n 0\rangle$ perpendicular to the state $S_+|0\rangle$. Following a similar orthogonalization procedure one can construct states with higher seniority. An iterative procedure is used to obtain the α_j [ref. [16])]. Given the α_j, the state with $J \neq 0$ can be obtained by diagonalizing the hamiltonian in a $\nu = 2$ configuration space. This generalized seniority basis offers an extremely powerful scheme for truncating the model space. For example, in the $N = 82$ isotones [17]), the maximum matrix to be diagonalized is only 9×9 in the $J = 2$ case. In spite of the extremely small basis, the results yield a good approximation to the full shell-model calculation [17]), for the energy levels and as we shall see later also for the E2 form factors. In principle, one could readjust the α_j for each J, but this has not been attempted. The hamiltonian for the generalized seniority model calculations consisted of a modified surface-δ interaction with an enhanced quadrupole component [17,18]) plus the single-particle energies given in table 1.

2.2. SHELL-MODEL CALCULATIONS FOR THE $N = 82$ ISOTONES

Shell-model calculations for $N = 82$ isotones with mass numbers $A = 133$–148 were carried out in the $g_{7/2}$-$d_{5/2}$-$s_{1/2}$-$d_{3/2}$-$h_{11/2}$ orbit space [12]). In order to constrain the state dimensionalities to less than 10 000 a truncation scheme was adopted which restricted the basis vectors to those which contained no more than four $h_{11/2}$ particles and which had seniorities no greater than 4. This truncation yields a reduction of approximately two orders of magnitude in the dimensions of states in the region of $A = 144$. The effective Hamiltonian was determined by a least-squares fit of the well-determined combinations of two-body matrix elements to experimental energy-level data in the $A = 133$–148 region. The initial values of the hamiltonian were calculated from a surface-delta parametrization.

With this space and interaction, energies of the experimentally established states in 134–146 are reproduced up to excitation energies of about 3 MeV in the even-mass systems and to 2 MeV in the odd-mass systems, with reproduction of high-spin

TABLE 1

Single particle energies used in the present calculations

	$N=82$	^{116}Sn and ^{110}Pd	
	ε_p (MeV)	ε_n (MeV)	ε_p (MeV)
$1h_{11/2}$	2.76	2.4	
$3s_{1/2}$	2.99	1.5	
$2d_{3/2}$	2.69	2.0	
$2d_{5/2}$	0.96	−0.5	6.48
$1g_{7/2}$	0.00	0.0	7.48
$1g_{9/2}$			1.60
$2p_{1/2}$			1.56
$2p_{3/2}$			0.20
$1f_{5/2}$			0.00

states continuing to higher excitation energies. The single-nucleon spectroscopic factors calculated with these wave functions are in excellent agreement with measured values for each of the orbits. In particular, the experimental evidence for increasing occupation of the $h_{11/2}$ orbit as $A=146$ is approached is reproduced.

We show in fig. 1 the calculated excitation energies of 2^+ states of the $N=82$ isotones from the generalized seniority scheme and from the shell model together with the experimental data. In general, both calculations reproduce the excitation energies of first 2^+ states. The shell-model results show slightly better agreement with experiment for the 2_2^+ and 2_3^+ states than the generalized seniority scheme results. The transition strengths for these states will be discussed in sect. 4.1.

3. The core-polarization effect on many-body wave function

We have proposed a prescription to improve the shell-model wave function in the framework of a microscopic theory [11]). Perturbation theory is applied to take into account the effects of the particle-hole giant resonances on the low-lying states. The effect can be regarded as a polarization of the core protons by the valence protons and neutrons through the proton-proton and proton-neutron two-body interactions. The perturbed single-particle wave function is given by;

$$|\tilde{\alpha}\rangle = |\alpha\rangle + \sum_{\beta}\sum_{\omega_\lambda} \frac{\langle(\beta\times\omega_\lambda)\alpha|V_{\rm ph}|\alpha\rangle}{[\varepsilon_\alpha-(\varepsilon_\beta+\omega_\lambda)]}|(\beta\times\omega_\lambda)\alpha\rangle\,, \tag{9}$$

where ω is the excitation energy of the giant resonance including both the discrete and continuum states. With this modified wave function, the reduced matrix element for the one-body operator is modified to be

$$\langle\tilde{\beta}\|\hat{T}_\lambda\|\tilde{\alpha}\rangle = \langle\beta\|\hat{T}_\lambda\|\alpha\rangle + \sum_{\omega_\lambda}[2\omega_\lambda/(\varepsilon_{\alpha\beta}^2-\omega_\lambda^2)]\langle V_{\rm ph}\rangle\langle\omega_\lambda\|\hat{T}_\lambda\|0\rangle/(2\lambda+1)^{1/2}\,, \tag{10}$$

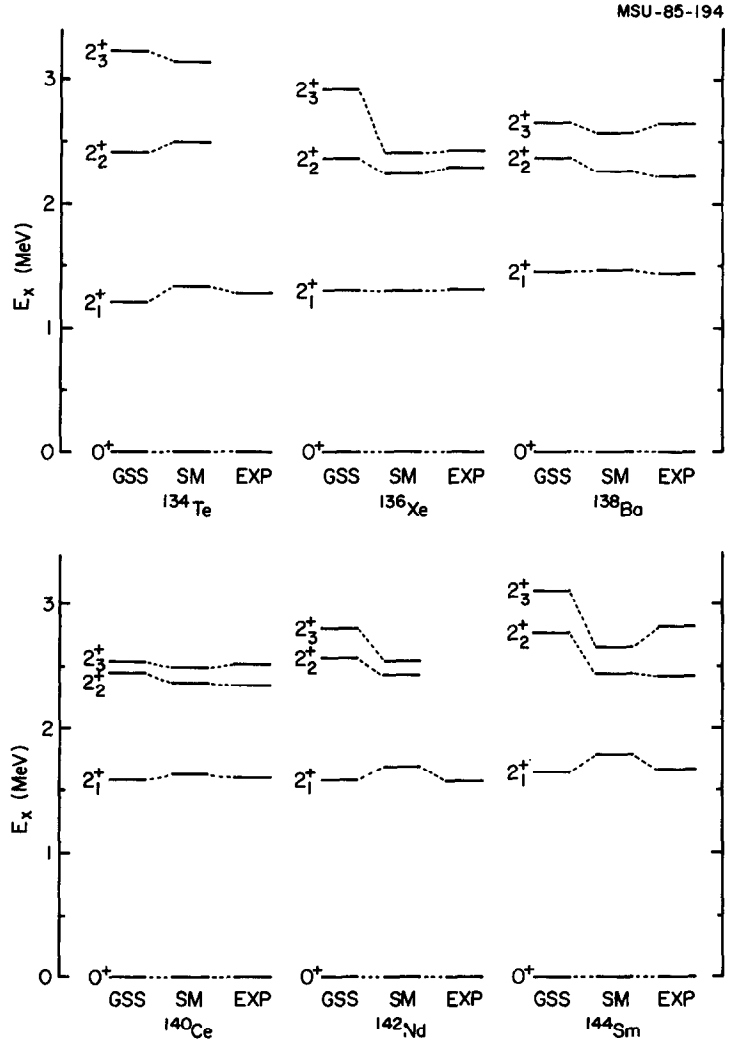

Fig. 1. The energy spectra of $N = 82$ isotones calculated by the generalized seniority scheme and the shell model. The experimental data are taken from ref. [19]).

where $\varepsilon_{\alpha\beta} = \varepsilon_\alpha - \varepsilon_\beta$. The reduced matrix element for the valence many-body wave function can be expressed in the form,

$$\langle J_f \| \hat{T}_\lambda \| J_i \rangle = \sum_{\alpha,\beta} C_{J_f,J_i}(\alpha, \beta) \langle \alpha \| \hat{T}_\lambda \| \beta \rangle , \tag{11}$$

where the states J_f and J_i are provided by the calculation of the generalized seniority scheme model (or the shell-model calculations) and $C_{J_f,J_i}(\alpha, \beta)$ are the structure factors (one-body transition densities) given by these calculations. The modified transition matrix element for the many-body wave functions is given by inserting

$\langle\tilde{\alpha}\|\hat{T}_\lambda\|\tilde{\beta}\rangle$ in eq. (11) in place of $\langle\alpha\|\hat{T}_\lambda\|\beta\rangle$:

$$\langle\tilde{J}_f\|\hat{T}_\lambda\|\tilde{J}_i\rangle = \sum_{\alpha,\beta} C_{J_f,J_i}(\alpha,\beta)\langle\tilde{\alpha}\|\hat{T}_\lambda\|\tilde{\beta}\rangle\,. \tag{12}$$

Note that the perturbed amplitudes in eqs. (10) and (12) take into account not only the first-order perturbation term but also the higher-order RPA corrections [6,20]).

4. Results

4.1. CORE-POLARIZATION CHARGES FOR THE $N=82$ ISOTONES

First we will discuss our results for the proton and neutron core-polarization charges due to the coupling to the giant resonances in the vicinity of $Z=62$ and $N=82$. The calculated strength distribution of the isoscalar (IS) and isovector (IV) giant resonances in ^{144}Sm are shown in fig. 2. The RPA response function was solved in coordinate space, taking into account the particle-escape width for a ^{144}Sm core [21]). The $N=82$ core is assumed to be a good closed-shell. The occupation probabilities of the protons in the five active orbits, determined from the result of the generalized seniority scheme calculations, are $N(1g_{7/2})=6.79$, $N(2d_{5/2})=3.16$, $N(2d_{3/2})=0.24$, $N(3s_{1/2})=0.06$ and $N(1h_{11/2})=1.75$, respectively. We used the Skyrme interaction SGII [9]) for the HF and RPA response calculations.

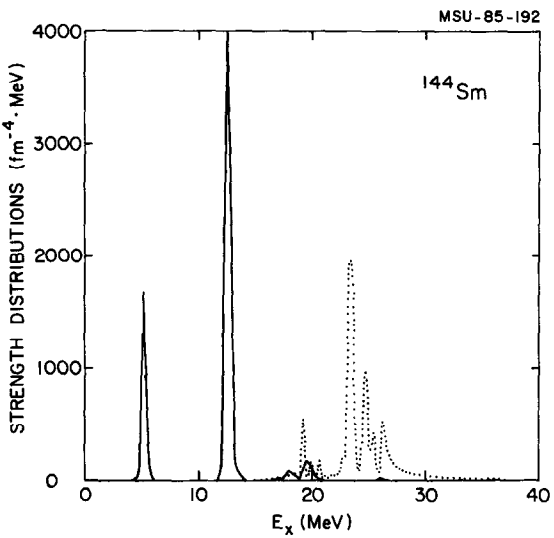

Fig. 2. RPA strength distributions for the isoscalar and isovector quadrupole operators in ^{144}Sm. The solid curve shows the result of the isoscalar operator, while the dashed curve corresponds to the isovector case. For the purpose of presentation the IS response is averaged over a gaussian shape with a width of 0.5 MeV. The calculated decay width of the IS response are 0.0 MeV and 0.1 MeV for the states at $E_x=5.2$ MeV and 12.6 MeV, respectively. No averaging was done for the IV response.

The isoscalar giant resonance has dominant peaks at 5.2 MeV and 12.6 MeV which exhaust, respectively, 8% and 79% of the energy-weighted sum rule. The isovector giant resonance is spread out in the energy region $E_x = 20$–30 MeV. The transition strengths in this energy region exhaust 77% of the IV energy-weighted sum rule. The isoscalar response has some transition strength in the energy region $E_x =$ 2–3 MeV (not shown in fig. 2), but they are discarded from the core polarization calculations since they are mainly due to the excitations within the $0\hbar\omega$ configuration space which are already included in the shell-model and the seniority-scheme calculations.

Fig. 3 shows the transition densities of the IS and IV giant resonances. The IS transition densities show surface peaks at 6 fm similar to the Tassie-type transition density [22]. The density function of the state at $E_x = 5.2$ MeV changes sign and has a minimum at about 4 fm, while the density function of the state at $E_x = 12.6$ MeV does not change sign but has a small shoulder in the interior. Similar radial dependences of the IS densities have been found for ^{208}Pb [ref. [23])]. The IV transition densities of the state at $E_x = 23.3$ MeV show a peak at $r = 4.5$ fm, which is 1.5 fm smaller than the location of the peaks for the IS states. While the shapes for the two IV states on the high energy side at $E_x = 23.3$ MeV and 24.8 MeV have some similarities to the IS shapes, the state at $E_x = 19.3$ MeV has a typical volume-type transition density which looks completely different from those of the IS states.

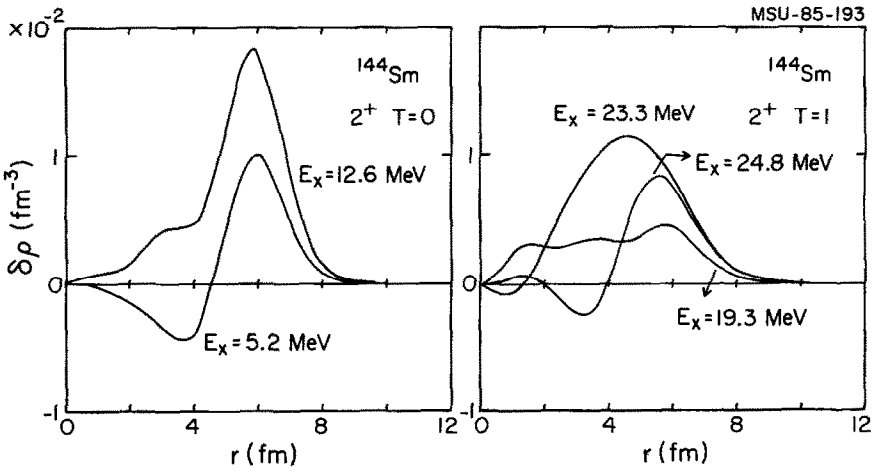

Fig. 3. The transition densities of IS and IV giant quadrupole states.

The calculated isoscalar and isovector core-polarization charges are given in table 2. The core-polarization charges for protons and neutrons are given by

$$\delta e_p = \delta e(\mathrm{IS}) - \delta e(\mathrm{IV}),$$
$$\delta e_n = \delta e(\mathrm{IS}) + \delta e(\mathrm{IV}). \qquad (13)$$

TABLE 2

Isoscalar and isovector E2 core polarization charges of single particle proton transitions in the vicinity of ^{144}Sm

α	β	$B(E2)_{s.p.}$ $(e^2 \cdot fm^4)$	δe(IS) ^{144}Sm core	δe(IS) ^{132}Sn core	δe(IV) ^{144}Sm core
$1g_{7/2}$	$1g_{7/2}$	75.9	0.527 (0.192)	0.548	0.168
$1g_{7/2}$	$2d_{5/2}$	4.8	0.836 (0.338)	0.860	0.143
$1g_{7/2}$	$2d_{3/2}$	75.7	0.794 (0.318)	0.818	0.145
$2d_{5/2}$	$2d_{5/2}$	67.5	0.600 (0.223)	0.624	0.141
$2d_{5/2}$	$2d_{3/2}$	26.1	0.601 (0.224)	0.626	0.140
$2d_{5/2}$	$3s_{1/2}$	161.2	0.617 (0.233)	0.641	0.125
$2d_{3/2}$	$2d_{3/2}$	63.2	0.600 (0.224)	0.627	0.139
$3s_{1/2}$	$2d_{3/2}$	54.9	0.620 (0.235)	0.645	0.123
$1h_{11/2}$	$1h_{11/2}$	105.5	0.628 (0.238)	0.650	0.159

The values in brackets in the fifth column are obtained from the IS state at $E_x = 5.2$ MeV. The $B(E2)_{s.p.}$ value is defined by $B(E2)_{s.p.} = |\langle \alpha \| \hat{T}_2 \| \beta \rangle|^2/(2j_\beta + 1)$ with the charges $e(\pi) = 1$.

The δe(IS) value is several times larger than the δe(IV) value reflecting the fact of larger and lower-energy isoscalar transition strengths relative to the isovector ones. There is some state dependence for the IS core-polarization charges, with values ranging from $\delta e = 0.5$ to 0.8. The IV values are more constant. Compared to the values of δe in the sd-shell nuclei [8]) the isoscalar δe for Sm region is somewhat larger because of the low-energy $0\hbar\omega$ type giant resonance at $E_x = 5.2$ MeV. The main configurations of this 5.2 MeV state are the $(1g_{9/2} \rightarrow 1g_{7/2})$ and $(1g_{9/2} \rightarrow 2d_{5/2})$ particle-hole (ph) neutron excitations which are outside of the shell-model configuration space. The IS core-polarization charges due to the state at $E_x = 5.2$ MeV are given in the fifth column in table 2 with brackets. This state contributes about 40% to the core-polarization charge. The core-polarization charge due to the $2\hbar\omega$-type excitation is about δe(IS) = 0.40 which is about 10% larger than that of the sd-shell. The δe(IV) are similar to those for the sd-shell.

In fig. 4, we show typical single-particle transition densities with and without the core-polarization corrections. In all cases, the core polarization increases the transition densities at the surface, but does not change the interior much. In the cases of the $(1g_{7/2} \rightarrow 2d_{3/2})$ and $(1g_{7/2} \rightarrow 2d_{5/2})$ transitions, the surface and the interior parts strongly cancel for the transition strength. Since the core-polarization affects only the surface part of the transition density, the transition strengths for these cases are more enhanced by the core polarization than the transitions with no sign change. This is the origin of the state dependence of the IS core polarization charge.

We have discarded the RPA strengths below 3 MeV from the core-polarization calculations discussed above. However, this procedure is not completely justified since some ph wave functions of $0\hbar\omega$-type giant resonance at 5.2 MeV might be mixed with the states below 3 MeV. In order to discuss this point more quantitatively, we performed RPA calculations for the IS quadrupole giant resonances in ^{132}Sn

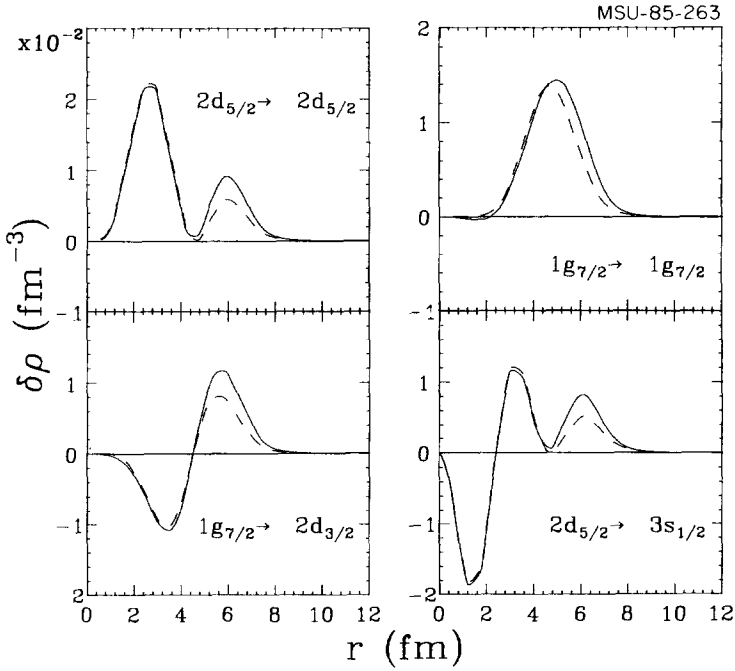

Fig. 4. The transition densities of single particle transitions in the vicinity of ^{144}Sm. The solid and dashed curves correspond to the case with and without core polarization, respectively.

assuming an $N = 82$ and $Z = 50$ core. In this case there is no transition strength below 3 MeV. Two collective states are found at the excitation energies at 4.4 MeV and 13.0 MeV with the transition strengths $B(E2) = 894\ e^2 \cdot \text{fm}^4$ and $2148\ e^2 \cdot \text{fm}^4$, respectively. These states exhaust 11% and 78% of the energy-weighted sum rule values, while the 2^+ states at $E_x = 5.2$ MeV and 12.6 MeV in ^{144}Sm exhaust 8% and 79% of the sum-rule value. The transition densities of the corresponding states are also found to have similar radial dependences. In table 2 we give the IS core-polarization charges calculated with eq. (10) for ^{144}Sm and ^{132}Sn. In both cases, the core-polarization charges show almost same state dependence and the values in ^{132}Sn are slightly larger than those of ^{144}Sm. These results can be easily understood since two giant resonances on both nuclei have similar excitation energies and transition densities.

4.2. C2 FORM FACTORS FOR THE $N = 82$ ISOTONES

The transition densities for the nine even-even nuclei from $A = 134$ to $A = 150$ are shown in figs. 5-7 for three lowest 2^+ states calculated by the generalized seniority scheme. The Coulomb (C2) form factors for four of these nuclei are also shown in

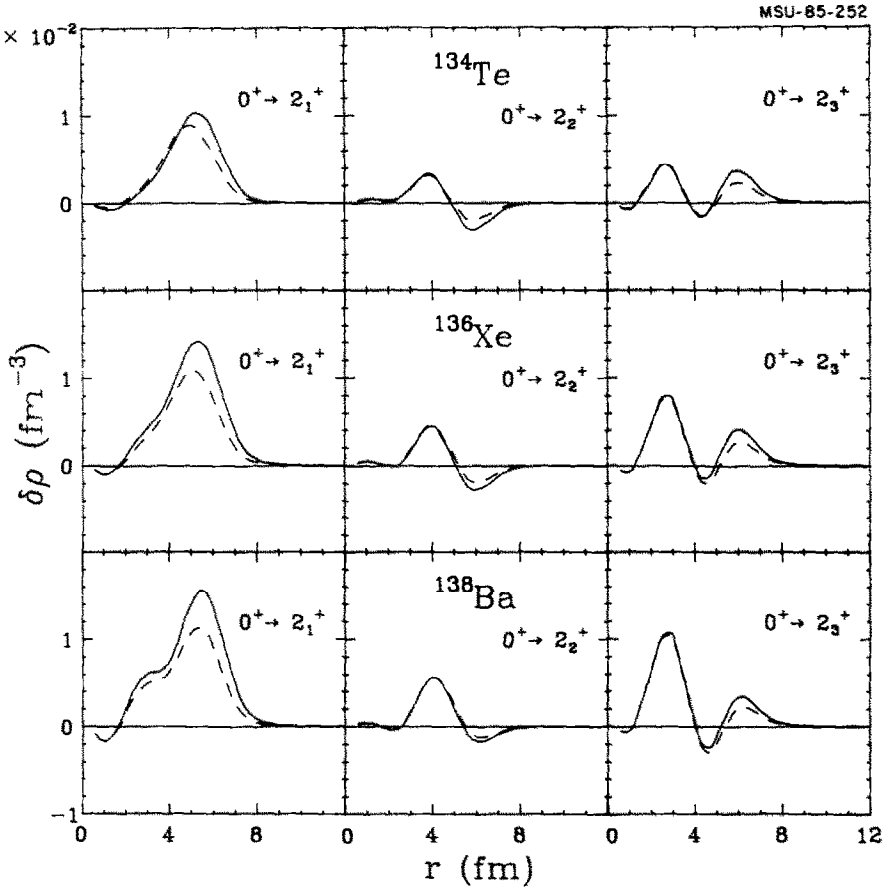

Fig. 5. The transition densities for the first three 2^+ states in ^{134}Te, ^{136}Xe and ^{138}Ba. The solid and dashed curves correspond to the case with and without core polarization, respectively.

fig. 8. The core polarization, in general, enhances the surface peak of the transition density irrespective of the shape of the valence transition density.

It is interesting to note that at the beginning of the shell the transition densities show a shape typical of the harmonic vibrator model [24]). Namely, the first 2^+ has a strong surface peak and the second one has two peaks with a sign change between the surface and the interior. The third 2^+ states show two peaks but with the same signs. However, this collective prediction is gradually violated in the heavier mass systems. Namely, the first 2^+ state in ^{138}Ba has a shoulder around 3 fm. This shoulder grows up gradually in the middle of the shell and becomes comparable to the surface peak in ^{142}Nd and ^{144}Sm. We notice also that the small dip around 1 fm becomes larger as a function of proton number.

In comparison with fig. 4, we can see that the first 2^+ state is dominated by the $1g_{7/2}$ configuration at the beginning of the shell. At around $A = 140$, the shoulder

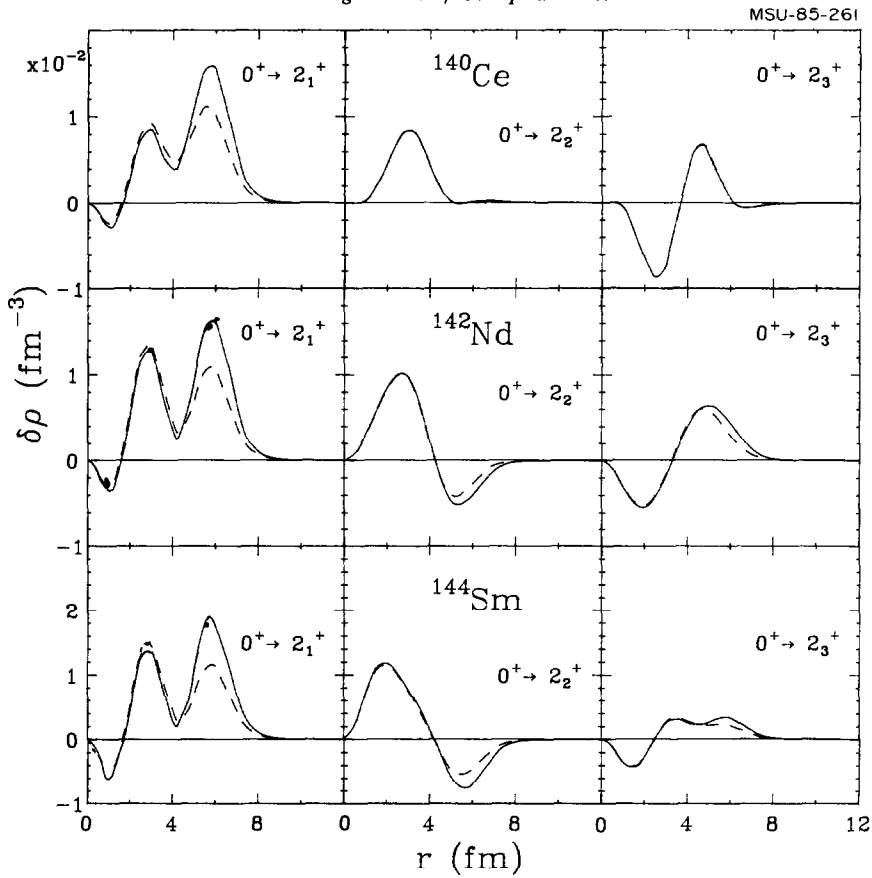

Fig. 6. The transition densities for the first three 2^+ states in ^{140}Ce, ^{142}Nd and ^{144}Sm. The solid and dashed curves correspond to the case with and without core polarization, respectively.

of the surface can be attributed to the amplitude of the $2d_{5/2}$ configuration. A large dip at the very interior of the transition densities for the 2_1^+ states in fig. 7 is due to the amplitude of the $3s_{1/2}$ configuration.

At the beginning of the shell the two peaks of the second 2^+ state have almost the same magnitude. The surface peak becomes smaller for increasing the mass number and disappears in ^{140}Ce. After that, the surface peak reappears again. The third 2^+ states can be classified into three categories. Namely, the third 2^+ states of the first three nuclei in fig. 5 have two peaks with same sign, while the next three nuclei in fig. 6 show two peaks with opposite sign. On the other hand, the last three nuclei in fig. 7 have one dominant peak at around $r = 2$ fm.

The E2 Coulomb form factors of several $N = 82$ isotones are shown in fig. 8. The first 2^+ state always has a dominant peak at a momentum transfer of $q = 0.5$ fm^{-1} and the second peak is about 2 orders of magnitude smaller than the first one. Information about the difference in the radial shape of the transition density for

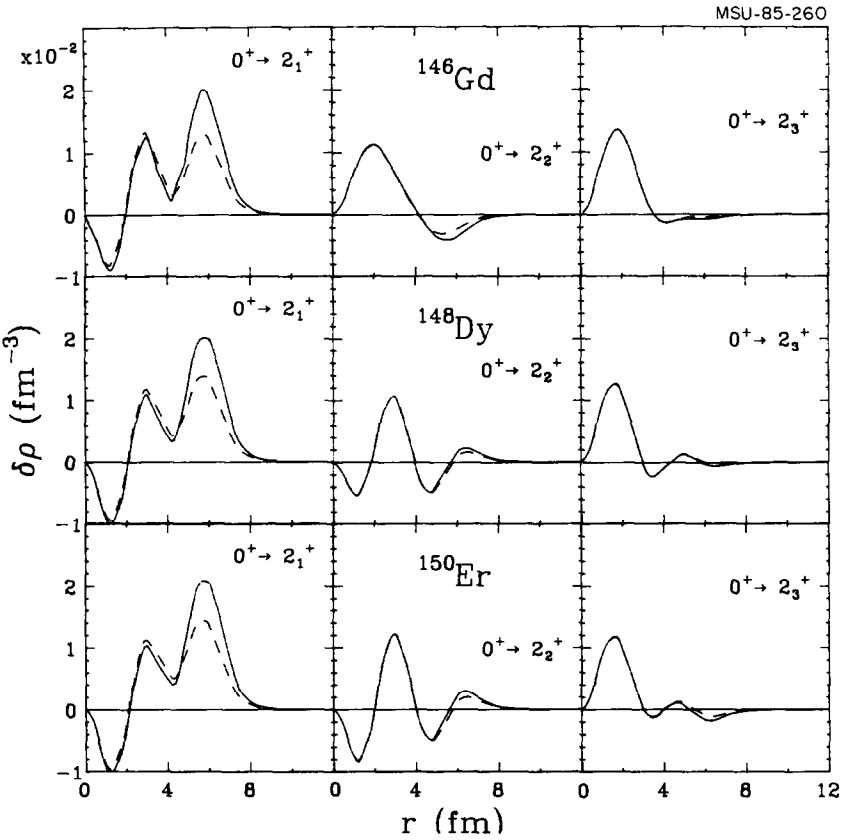

Fig. 7. The transition densities for the first three 2^+ states in ^{146}Gd, ^{148}Dy and ^{150}Er. The solid and dashed curves correspond to the case with and without core polarization, respectively.

the 2_1^+ state might be obtained from the magnitudes of the second and the third peaks in fig. 8. For the second and third 2^+ states, the first and the second peaks in the form factors are more similar in magnitude. Clearly the detailed q-dependence of the experimental form factor, especially at $q = 1$–2 fm^{-1}, is needed in order to distinguish between the different types of the transition densities which are shown in figs. 5–7.

We have also studied the transition densities of $N = 82$ isotones using the shell-model wave functions. Some results obtained with the shell-model wave function are shown in figs. 9 and 10 in comparison with those of the generalized seniority scheme. In general, the two calculations show quite similar results for the transition densities and the B(E2) values. For nuclei with $A = 134$–140, the B(E2) values of the first 2^+ states are very similar (see fig. 11). There are appreciable differences in the transition strengths and densities between the two calculations in the cases of ^{144}Sm and ^{146}Gd. For ^{144}Sm (see fig. 10) the shape of the transition densities are very similar to each other, however the generalized seniority scheme result is

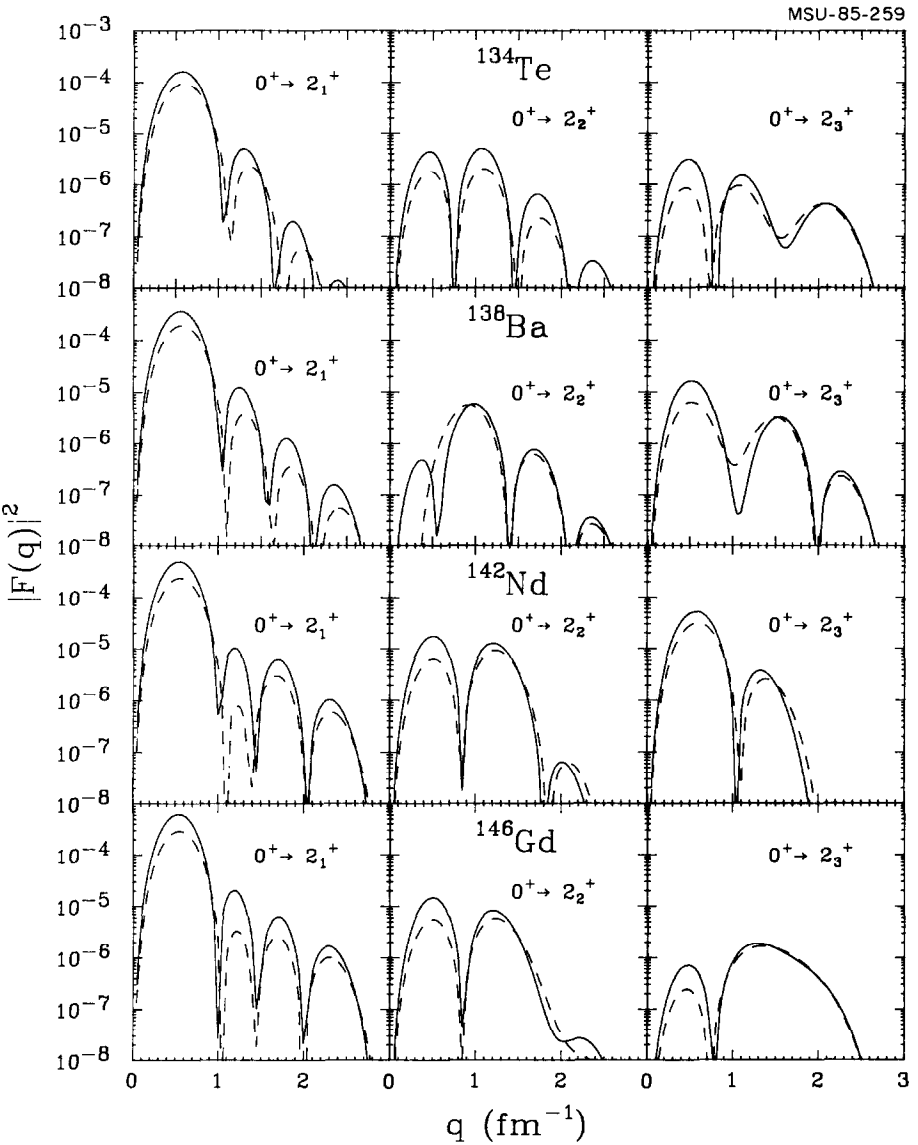

Fig. 8. The Coulomb form factor for the first three 2^+ states in ^{134}Te, ^{138}Ba, ^{142}Nd and ^{146}Gd. The solid and dashed curves correspond to the case with and without core polarization, respectively. The center-of-mass correction was taken into account in the harmonic oscillator approximation [26]), while the nucleon finite size corrections were incorporated in the dipole approximation [25]).

somewhat larger in magnitude than that of the shell model. B(E2) values for the second 2^+ states are also very similar for $A = 134$–142 with the exception of ^{138}Ba. This difference in ^{138}Ba is clearly seen in the surface part of the transition density as is shown in fig. 9. The B(E2) values from the shell-model calculation in fig. 11 show a kink at ^{144}Sm similar to the experimental values, while the results of the

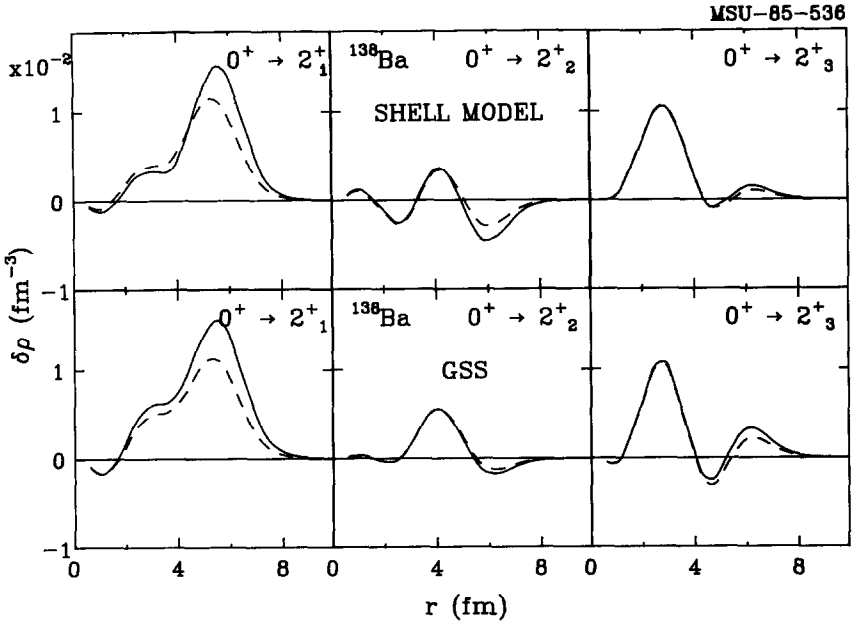

Fig. 9. The calculated transition densities for the first three 2^+ states in ^{138}Ba. The solid and dashed curves correspond to the case with and without the core polarization, respectively.

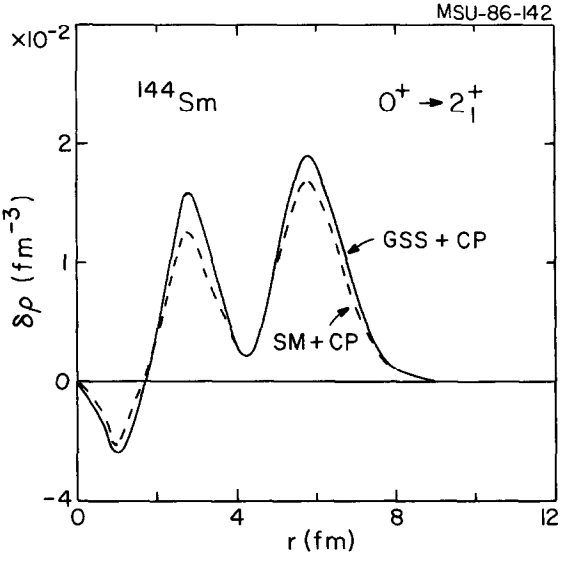

Fig. 10. The calculated transition densities for the first 2^+ state in ^{144}Sm obtained in the generalized seniority scheme (solid curve) and the shell model (dashed curve), both including the core polarization.

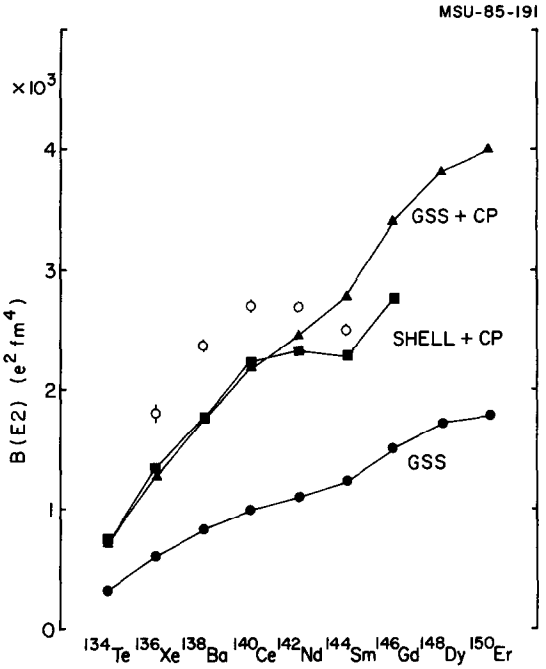

Fig. 11. The $0_1^+ \to 2_1^+$ B(E2) values for the $N = 82$ isotones. The calculated results are obtained by the generalized seniority scheme (triangles) and the shell model (squares) with core polarization. The results of the generalized seniority scheme without core polarization (filled circles) are also plotted. The data (open circles with error bars) are taken from ref. [28]).

generalized seniority scheme show a nearly linear increase in the B(E2) values with respect to the mass number.

The calculations which include core polarization greatly improve the agreement with the experimental B(E2) values as shown in fig. 11. However, our results are still 10–20% smaller than the experimental ones. This difference should not change the general character of the transition density since it is small in terms of an increase in the effective charge, 0.05–0.1. Experimental information on the longitudinal form factor to the first 2^+ states as well as to the second and the third 2^+ states is needed for a complete test of our model. It would also be interesting to have experimental information on the B(E2) value to the 2_1^+ state in ^{146}Gd where the shell model and the generalized scheme give an appreciable difference.

In the generalized seniority model, the reduction formulae of the transition strength can be expressed in terms of a Clebsch-Gordan coefficient [27]):

$$B(\mathrm{E2}) = \frac{1}{2J_i+1} \left|\langle n\nu_f;\, J_f \| \hat{T}(\mathrm{E2}) \| n\nu_i;\, J_i\rangle\right|^2$$

$$= \frac{1}{2J_i+1} \left(\tfrac{1}{2}(\Omega-\nu_i), \tfrac{1}{2}(n-\Omega), 1, 0 \,|\, \tfrac{1}{2}(\Omega-\nu_f), \tfrac{1}{2}(n-\Omega)\right)^2$$

$$\times \left|\langle n = 2\nu_f \| \hat{T}(\mathrm{E2}) \| n = 2\nu_i\rangle\right|^2 . \qquad (14)$$

The n-dependence of the $B(E2)$ value from the first 2^+ state ($\nu = 2$) to the ground state ($\nu = 0$) is thus given by

$$B(E2; 0^+ \to 2^+) \propto (\Omega - \tfrac{1}{2}n)\tfrac{1}{2}n \tag{15}$$

and the n-dependence of the $B(E2)$ value from the first 4^+ state ($\nu = 2$) to the first 2^+ state is proportional to

$$B(E2; 4_1^+ \to 2_1^+) \propto (n - \Omega)^2 , \tag{16}$$

where n is the number of the particles outside of the $Z = 50$ core. When both $Z = 50$ and $Z = 64$ are considered as good closed-shells, $\Omega = 7$. Eq. (15) shows that the $B(E2; 0^+ \to 2_1^+)$ has a maximum in the middle of the shell and decreases at the beginning and the end of the shell. The $B(E2)$ values in fig. 11 obtained by microscopic models follows this simple formula at the beginning of the shell. The kink in the $B(E2)$ value at ^{144}Sm certainly suggests the sub-shell closure of $Z = 64$ in the shell-model calculation and the experiment. The $B(E2; 4_1^+ \to 2_1^+)$ values calculated by the generalized seniority scheme are shown in fig. 12 together with some experimental data. The rapid decrease of the $B(E2)$ implies that the wave functions of the 4_1^+ states are dominated by seniority $\nu = 2$.

4.3. C2 FORM FACTORS FOR THE Sn ISOTOPES

The calculated core polarization charges in the vicinity of ^{116}Sn are listed in table 3. The IS and IV quadrupole states are calculated assuming $Z = 50$ and $N = 66$ as a closed core. The state dependences of the δe values for the neutrons in table 3 are similar to those for protons in table 1. However, the average values of δe in table 3 are about 20% smaller than those of table 2 (15% for δe(IS) and 25% for

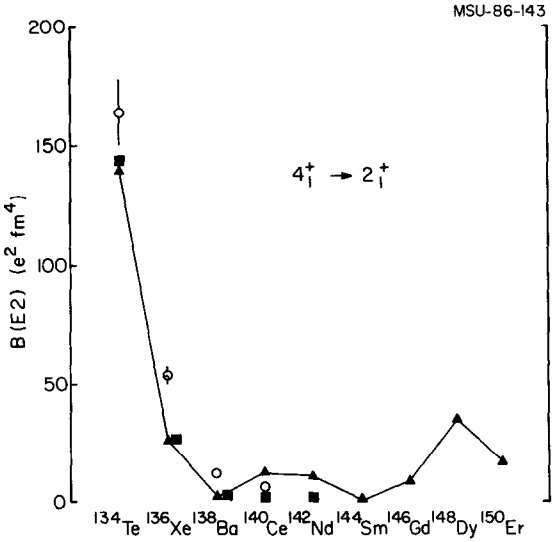

Fig. 12. The $4_1^+ \to 2_1^+$ $B(E2)$ values for the $N = 82$ isotones. The calculated results are obtained by the generalized scheme (triangles) and the shell model (squares) with core polarization. The data (open circles with error bars) are taken from ref. [29]).

TABLE 3

Isoscalar and isovector E2 core polarization charges of single-particle transitions in the vicinity of ^{116}Sn

	α	β	$B(E2)_{s.p.}$ ($e^2 \cdot fm^4$)	δe (IS)	δe (IV)
ν	$1g_{7/2}$	$1g_{7/2}$	60.11	0.504	0.130
	$2d_{5/2}$	$1g_{7/2}$	3.32	0.703	0.106
	$2d_{3/2}$	$1g_{7/2}$	34.81	0.670	0.106
	$2d_{5/2}$	$2d_{5/2}$	57.26	0.520	0.108
	$2d_{3/2}$	$2d_{5/2}$	15.05	0.517	0.106
	$3s_{1/2}$	$2d_{5/2}$	47.38	0.518	0.092
	$2d_{3/2}$	$2d_{3/2}$	55.97	0.513	0.104
	$3s_{1/2}$	$2d_{3/2}$	49.96	0.515	0.089
	$1h_{11/2}$	$1h_{11/2}$	83.61	0.574	0.122
π	$1f_{5/2}$	$1f_{5/2}$	42.62	0.446	0.139
	$2p_{3/2}$	$1f_{5/2}$	5.51	0.664	0.124
	$2p_{1/2}$	$1f_{5/2}$	20.83	0.643	0.125
	$2p_{3/2}$	$2p_{3/2}$	35.55	0.563	0.134
	$2p_{1/2}$	$2p_{3/2}$	35.81	0.562	0.134
	$1g_{9/2}$	$1g_{9/2}$	67.31	0.548	0.131
	$1g_{7/2}$	$1g_{9/2}$	4.70	0.533	0.129
	$2d_{5/2}$	$1g_{9/2}$	37.57	0.706	0.106
	$1g_{7/2}$	$1g_{7/2}$	63.93	0.516	0.127
	$2d_{5/2}$	$1g_{7/2}$	3.59	0.696	0.102
	$2d_{5/2}$	$2d_{5/2}$	61.55	0.506	0.103

The $B(E2)_{s.p.}$ value is defined by $B(E2)_{s.p.} = |\langle\alpha|\hat{T}_2|\beta\rangle|^2/(2j_\beta+1)$ with the changes $e(\pi) = e(\nu) = 1$.

δe(IV)). For the ^{116}Sn case, the average neutron core polarization charge is $\delta e_n \approx 0.65$, and the average proton core polarization charge is $\delta e_p \approx 0.44$.

We have studied three 2^+ states in ^{116}Sn. The wave functions were obtained from the generalized seniority scheme calculations using the modified surface-δ interaction with an enhanced quadrupole component [17,18]) and the single particle energies from table 1. The transition density of the first 2^+ states at $E_x = 1.38$ MeV is shown in fig. 13. Since shell-model amplitudes for the proton configurations for these states vanish, the transition densities are determined only by the core polarization and show similar surface peaks to the IS giant resonances (see fig. 3). The calculated B(E2) value for the first 2^+ state in ^{116}Sn is 616.8 $e^2 \cdot fm^4$. This experimental value corresponds to an empirical effective charge of $\delta e_n \approx 1.2$. The experimental B(E2) value is larger, 2120 ± 250 $e^2 \cdot fm^4$. The Coulomb form factor for the first 2^+ state is shown in fig. 14 in comparison with the experimental data.

4.4. C2 FORM FACTORS FOR ^{110}Pd

As an example of the application of our model to more complicated nuclei, in which both protons and neutrons are active, we will discuss the 2^+ states in ^{110}Pd.

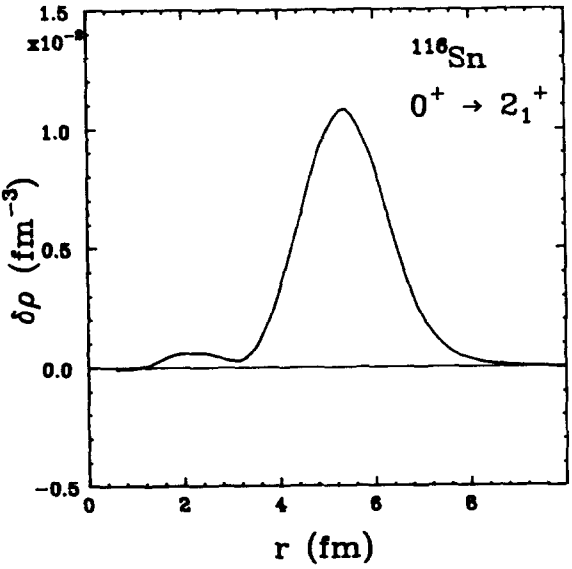

Fig. 13. The transition density for 2^+ states in ^{116}Sn. The solid and dashed curves correspond to the case with and without core polarization, respectively.

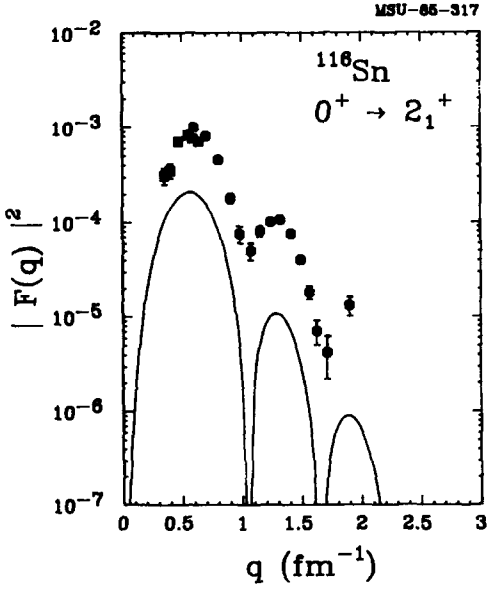

Fig. 14. The Coulomb form factors for 2^+ state in ^{116}Sn. The solid and dashed curves correspond to the case with and without core polarization, respectively. The data are taken from ref. [30]).

The many-body wave functions are obtained in two steps. First the generalized seniority scheme is used to calculate the proton and neutron bosons separately as is described in sect. 3. These results are then combined with the results of IBA-2 calculations to yield the observed transition density. The approach is similar to that used first by Dieperink [31]) to predict the transition densities in ^{150}Nd.

In the IBA model the E2 transition operator can be written as

$$T^{\mathrm{E2}} = \alpha_\lambda (s_\lambda^\dagger d_\lambda + d_\lambda^\dagger s_\lambda)^{(2)} + \beta_\lambda (d_\lambda^\dagger d_\lambda)^{(2)}, \qquad \lambda = \nu, \pi .$$

In the calculation of E2 transition amplitudes, the coefficients α_λ and β_λ are taken as constants, where α_λ plays the role of the neutron (proton) boson effective charges and $\chi_\lambda = \beta_\lambda / \alpha_\lambda$ is a parameter that enters also in the description of the IBA-2 hamiltonian. For the calculation of transition densities this approach is generalized, and α_λ and β_λ are considered to be a function of r, i.e.

$$\rho_{\mathrm{if}}(r) = \alpha_\lambda(r) \langle \mathrm{f} | (s_\lambda^\dagger d_\lambda + d_\lambda^\dagger s_\lambda)^{(2)} | \mathrm{i} \rangle + \beta_\lambda(r) \langle \mathrm{f} | (d_\lambda^\dagger d_\lambda)^{(2)} | \mathrm{i} \rangle .$$

The matrix elements in this expression can readily be calculated from the IBA-2 wave functions, and are the same as those that enter into the calculation of E2 transitions. The boson densities $\alpha(r)$ and $\beta(r)$ can be calculated from the microscopic structure of the s- and d-bosons, which in turn are defined via the equivalence relations

$$|s^N\rangle \sim S_+^N |0\rangle = |\tilde{j}^{2N} w = 0, J = 0\rangle ,$$

$$|s^{N-1} d\rangle \sim S_+^{N-1} D |0\rangle = |\tilde{j}^{2N} w = 2, J = 2\rangle ,$$

where the lowest $J = 2$ state corresponds to the d-boson. We can therefore now write

$$\alpha(r) = \langle \tilde{j}^{2N} w = 0, J = 0 \| \mathrm{E2} \| \tilde{j}^{2N} w = 2, J = 2 \rangle / \sqrt{5} ,$$

$$\beta(r) = \langle \tilde{j}^{2N} w = 0, J = 2 \| \mathrm{E2} \| \tilde{j}^{2N} w = 2, J = 2 \rangle / \sqrt{2} .$$

These matrix elements can be calculated following the procedure given in sect. 3.

We have applied this procedure to ^{110}Pd where extensive electron scattering data are available [33]). In the IBA calculation we used the parameters given in ref. [32]). The calculations with bare charges give the $B(\mathrm{E2})$ values 445 $e^2 \cdot \mathrm{fm}^4$ for the 2_1^+ state, 25.6 $e^2 \cdot \mathrm{fm}^4$ for the 2_2^+ state and 1.71 $e^2 \cdot \mathrm{fm}^4$ for the 2_3^+ state, while the experimental values are $B_{\mathrm{exp}}(\mathrm{E2}) = 9100 \pm 600$ $e^2 \cdot \mathrm{fm}^4$ (for 2_1^+) and 134 ± 24 $e^2 \cdot \mathrm{fm}^4$ (for 2_2^+) [ref. [29])]. The $B(\mathrm{E2})_{\mathrm{exp}}$ for 2_3^+ state is not yet reported. The $B(\mathrm{E2})$ values are increased by the core-polarization effect to be 3620 $e^2 \cdot \mathrm{fm}^4$ (for 2_1^+), 189 $e^2 \cdot \mathrm{fm}^4$ (for 2_2^+) and 5.21 $e^2 \cdot \mathrm{fm}^4$ (for 2_3^+). We note that the contribution which arises from the polarization of the core protons by the valence neutrons accounts for about half of the total transition matrix element.

The transition densities and the Coulomb form factors of these 2^+ states are shown in figs. 15 and 16. The core polarization increases the transition density of

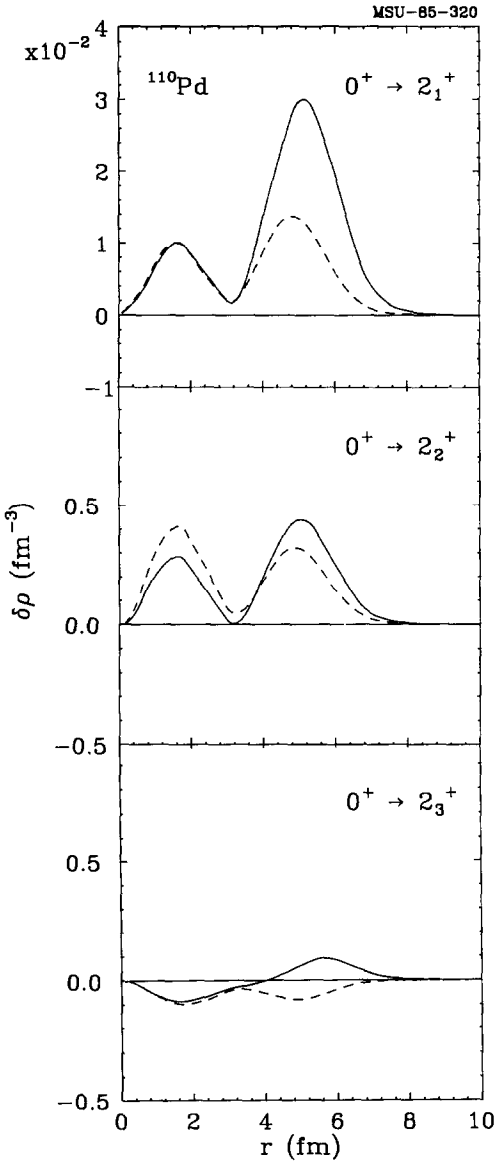

Fig. 15. The transition densities for 2^+ states in ^{110}Pd. The solid and dashed curves correspond to the case with and without core polarization, respectively.

the 2_1^+ state in the surface region by almost a factor of three, but the interior part changes very little. This increase of the surface peak creates a difference of a factor of eight between the calculated $B(E2)$ values with and without core polarizations. The Coulomb form factor for the first 2^+ state is also enhanced almost an order of magnitude compared to the result without the core polarizations. The positions of

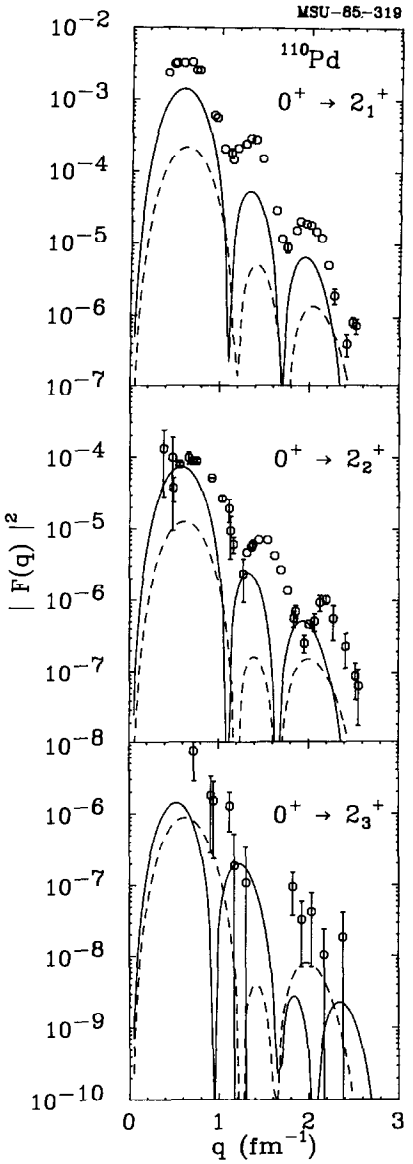

Fig. 16. The Coulomb form factors for 2^+ states in ^{110}Pd. The solid and dashed curves correspond to the case with and without core polarization, respectively. The data are taken from ref. [32]).

three peaks and the minima are well-reproduced by the calculation having the core polarizations. However, the absolute magnitudes of the calculated form factor is still smaller than the experimental ones. For the second 2^+ state, the core polarization increases the surface peak again and decreases the height of interior peak. On the other hand, the surface peak of the third 2^+ state changes sign due to the coupling

to the giant resonances, while the interior is not changed. The calculated form factor for the second 2^+ state is very close to the experimental data in absolute magnitude at the first peak, but the peak positions are slightly shifted. The form factor for the third 2^+ state is also shown in fig. 16, but it is difficult to compare with the data because of the poor statistics of the data.

5. Summary

We have studied the effect of core-polarization on the electric quadrupole transitions in medium-heavy nuclei. The self-consistent HF and RPA methods were used for calculations of the single-particle wave functions and the response functions of IS and IV giant resonances. All calculations made use of the Skyrme-type interaction SGII. We calculated the many-body wave functions by using the generalized seniority scheme with the surface-δ interaction. The results of the large-scale shell-model calculations with phenomenological two-body matrix elements were also discussed in the case of the $N = 82$ isotones. For the matrix elements involved in the multi-particle transitions we obtained average IS and IV effective charges $\delta e(\mathrm{IS}) \cong 0.6$ and $\delta e(\mathrm{IV}) \cong 0.1$.

The transition densities of the 2^+ states of $N = 82$ isotones show a typical feature of the harmonic vibration at the beginning of the shell. However this picture is modified in the nuclei $A > 140$ because of the appreciable contributions of the $2d_{5/2}$ and $3s_{1/2}$ configurations to the first 2^+ state. The $B(\mathrm{E2})$ values of $N = 82$ isotones are increased by the core-polarization effects typically by a factor of two, but are still 10–20% smaller than the experimental values. The calculated $B(\mathrm{E2})$ values based on the shell-model wave functions show a kink at ^{144}Sm in agreement with the experimental data, suggesting a sub-shell closure at $Z = 64$; while the generalized seniority scheme gives a linear increase of the $B(\mathrm{E2})$ values. We showed in fig. 8 the Coulomb form factors of several $N = 82$ isotones. Experimental data for these transitions are needed.

The quadrupole transitions in ^{116}Sn and ^{110}Pd were also studied by using the same microscopic model. In ^{116}Sn, the transition strength is entirely determined by the core-polarization charges due to the proton–neutron interaction between the valence neutrons and the protons in the core. The $B(\mathrm{E2})$ value of the first 2^+ state in ^{110}Pd has almost equal contributions from neutron and proton amplitudes and is enhanced by the core polarization by a factor of about 10. However, in both cases, the experimental data are still 2–3 times larger than our calculated values. Our microscopic description of these transitions thus is still incomplete. We speculate that the problem may be associated with the splitting of the "$\Delta\hbar\omega = 0$" E2 mode into two parts; (1) the low-lying state around $E_x = 1.5$ MeV and (2) the high-lying state which we calculate to be at about $E_x = 5$ MeV for $N = 82$ and Sn and to have $B(\mathrm{E2})$ $(0 \rightarrow 2)$ values at $840\, e^2 \cdot \mathrm{fm}^4$ and $420\, e^2 \cdot \mathrm{fm}^4$, respectively. Perhaps in reality these two states are mixed differently than in our calculations. In this regard, it would be

interesting to have an experimental confirmation of the E2 strength expected in the region of $E_x = 5$ MeV.

This research was supported in part by the National Science Foundation under grant nos. PHY-83-12245 and PHY-85-09736.

References

1) J. Heisenberg, Adv. Nucl. Phys. **12** (1981) 1, and references therein
2) S. Cohen and D. Kurath, Nucl. Phys. **73** (1965) 1
3) B.A. Brown, R. Radhi and B.H. Wildenthal, Phys. Reports **C101** (1984) 213
4) T. Iwamoto, H. Horie and A. Yokoyama, Phys. Rev. **C5** (1982) 658
5) M. Rho, Nucl. Phys. **65** (1965) 497;
M. Waroquier and K. Heyde, Nucl. Phys. **A164** (1971) 113
6) A. Bohr and B.R. Mottelson, Nuclear structure, vol. II (Benjamin, Mass., 1979)
7) Y. Horikawa, T. Hoshino and A. Arima, Nucl. Phys. **A228** (1977) 297;
F. Petrovich, H. McManus, J. Borysowicz and G.R. Hammerstein, Phys. Rev. **C16** (1977) 839
8) H. Sagawa and B.A. Brown, Nucl. Phys. **A430** (1984) 84
9) Nguyen van Giai and H. Sagawa, Phys. Lett. **106B** (1981) 379
10) I. Hamamoto, Phys. Reports **10C** (1974) 1;
T. Suzuki, Nucl. Phys. **A217** (1973) 182; **A220** (1974) 569
11) H. Sagawa and B.A. Brown, Phys. Lett. **150B** (1985) 247
12) H. Kruse and B.H. Wildenthal, unpublished
13) V. Gillet, B. Giraud and M. Rho, Phys. Rev. **178** (1969) 1695
14) O. Scholten, an Invited Talk at Gull Lake Workshop on Interacting boson-boson and boson-fermion systems (1984, May) p. 260
15) I. Talmi, Nucl. Phys. **A172** (1971) 1
16) O. Scholten, Phys. Rev. **C28** (1983) 1783
17) O. Scholten and H. Kruse, Phys. Lett. **125B** (1983) 113
18) P.J. Brussard and P.W.M. Glaudemans, Shell-model applications in nuclear spectroscopy (North-Holland, Amsterdam, 1977) p. 106
19) Table of Isotopes, ed. C.M. Lederer and V.S. Shirley, 1978
20) S. Yoshida and L. Zamick, Ann. Rev. Nucl. Sci. **22** (1972) 121
21) G.F. Bertsch and S.F. Tsai, Phys. Reports **18** (1975) 125;
S. Shlomo and G.F. Bertsch, Nucl. Phys. **A243** (1975) 307
22) L.J. Tassie, Australian J. Phys. **9** (1956) 407
23) H. Sagawa and Nguyen van Giai, Phys. Lett. **127B** (1983) 393
24) K. Hosoyama, Y. Torizuka, Y. Kawazoe and H. Ui, Proc. of the Int. Conf. on Nuclear structure studies using electron scattering and photoreaction (1972, Sendai) p. 139
25) A. Bohr and B.R. Mottelson, Nuclear structure, vol. I (Benjamin, Mass., 1975) p. 386
26) L.J. Tassie and F.C. Baker, Phys. Rev. **111** (1958) 940
27) M. Ichimura, Progress in Nucl. Phys. **10** (1969) 307;
O. Scholten and S. Pittel, Phys. Lett. **120B** (1983) 9
28) L.-O. Edvardson and L.O. Norlin, unpublished (1975);
G. Kindleben and T.W. Elze, Z. Phys. **A286** (1978) 415;
D. Eccleshall, M.J.L. Yates and J.J. Simpson, Nucl. Phys. **78** (1966) 481;
P.R. Christensen, I. Chernov, E.E. Gross, R. Stokstad and F. Videbaek, Nucl. Phys. **A207** (1973) 433
29) K. Kawade, G. Battistuzzi, H. Lawin, K. Sistemich and J. Blomqvist, Z. Phys. **A298** (1980) 187;
J.A. Morman, W.C. Schick, Jr. and W.L. Talbert, Jr., Phys. Rev. **C11** (1975) 913;
W.M. Currie, Nucl. Phys. **48** (1963) 561;
J. Burde, G. Engler, A. Molchadzki, A. Ginsburg and I. Unna, Jahresberichte (1966, Max-Planck-Inst., Heidelberg);

P. Kleinheinz, M.R. Maier, R.M. Diamond, F.S. Stephens and R.K. Sheline, Phys. Lett. **B53** (1975) 442

30) P.X. Ho, J.B. Bellicard, Ph. Leconte and I. Sick, Proc. of the Int. Conf. on Nuclear structure studies using electron scattering and photoreaction, Sendai, 1972, ed. K. Shoda and H. Ui, p. 125
31) A.E.L. Dieperink, F. Iachello, A. Rinat and C. Creswell, Phys. Lett. **76B** (1985) 135
32) P. Van Isacker and P. Puddu, Nucl. Phys. **A348** (1980) 125
33) J.B. Van Der Laan, A.J.C. Burghardt, C.W. De Jager and H. De Vries, Phys. Lett. **153B** (1985) 130